

## Article

# A Novel Geo-Social-Aware Video Edge Delivery Strategy Based on Modeling of Social-Geographical Dynamic in an Urban Area

Shijie Jia <sup>1</sup>, Yan Cui <sup>2</sup> and Ruiling Zhang <sup>1,\*</sup><sup>1</sup> Academy of Information Technology, Luoyang Normal University, Luoyang 471934, China<sup>2</sup> Department of Open Education, Luoyang Radio and Television University, Luoyang 471003, China

\* Correspondence: ruilingzhang@163.com

**Abstract:** Social networks change the way and approaches of video spread and promote range and speed of video spread, which results in frequent traffic blowout and a heavy load on the networks. The social and geographical communication efficiency determines the efficiency of video sharing, which enables the eruptible traffic to be offloaded in underlying networks to relieve the load of networks and ensure the user quality of the experience. In this paper, we propose a novel geo-social-aware video edge delivery strategy based on the modeling of the social-geographical dynamic in urban area (GSVD). By investigating the frequency of sharing behaviors, social communication efficiency, and efficiency of social sub-network consisting of one-hop social neighbors of users, GSVD estimates the interactive and basic social relationship to calculate the closeness of the social relationship between mobile users. GSVD makes use of grid partition and coding subarea to express the geographical location of mobile users and designs a calculation method of coding-based geographical distance. GSVD considers the dynamic update of social distance and geographical location and designs a measurement of video delivery quality in terms of delivery delay and playback continuity. A strategy of video delivery with the consideration of adapting to social-geographical dynamic is designed, which effectively promotes the efficiency of video sharing. Extensive tests show how GSVD achieves much better performance results in comparison with other state of the art solutions.

**Keywords:** social influence; geographical distance; video delivery; video quality



**Citation:** Jia, S.; Cui, Y.; Zhang, R. A Novel Geo-Social-Aware Video Edge Delivery Strategy Based on Modeling of Social-Geographical Dynamic in an Urban Area. *Electronics* **2022**, *11*, 4230. <https://doi.org/10.3390/electronics11244230>

Academic Editor: Wojciech Mazurczyk

Received: 31 October 2022

Accepted: 10 December 2022

Published: 19 December 2022

**Publisher's Note:** MDPI stays neutral with regard to jurisdictional claims in published maps and institutional affiliations.



**Copyright:** © 2022 by the authors. Licensee MDPI, Basel, Switzerland. This article is an open access article distributed under the terms and conditions of the Creative Commons Attribution (CC BY) license (<https://creativecommons.org/licenses/by/4.0/>).

## 1. Introduction

The development and application of wireless communication technologies (e.g., 5G/6G) not only support the ubiquitous access of mobile users to break time and space constraints, but also provide enough network bandwidth for various applications with a high requirement of bandwidth [1–4]. Video services such as IPTV, VoD, and video living rely on wonderful content and quality of services (QoS) and have become the most popular application on the Internet, so much so that video traffic has become more than 70% of the world's total traffic [5–8]. The combination between video applications and social networks promotes the process and range of video dissemination because the video spread considers social links between users as the new sharing channel [9–13]. The assistance of social networks further results in the blowout of video traffic, which brings a heavy burden for the core networks. In particular, the high density of a population in a city promotes social efficiency, so that the traffic load of social-based video sharing in a city is much higher than that of other video application scenes [14]. The high traffic load aggravate congestion levels of networks, which results in a high loss rate of video data and reduces user quality of experience (QoE) [15–17]. The high-efficiency video delivery effectively relieves the traffic load of networks by investigating the social relationships and geographical locations of mobile users to implement traffic offloading in underlying networks [18]. The combined measurement of social relationships and geographical locations is crucial for the performance and QoS of social-based video delivery.

The closeness levels and interaction efficiency of social relationship between users determine the influence levels for speed and range of video dissemination, which further

influences the performance of video delivery and user QoE. The comprehensive measurement for the characteristics of closeness and interaction is very important for estimating the accuracy of closeness levels and the interaction efficiency of social relationships. On the other hand, the dynamic of geographical location caused by the mobility of mobile users brings a severely negative influence for the performance of video delivery due to the frequent variation of transmission paths of video data. The accurate expression and low-cost update of the dynamic geographical location of mobile users in an urban area is also very important for the estimation of the geographical distance between mobile users. Numerous researchers focus on optimization of the QoE-driven performance of video delivery with social assistance [19–25]. For instance, Cao et al. propose social-aware D2D-based video multiCast system by investigation of the cooperation between mobile users to implement cooperative video multicast and allocate D2D radio resources [19]. Hung et al. propose an optimization method of live video streaming services in mobile edge computing by adjustment of the backhaul capacity and allocation of the caching space of an edge-enabled cellular system to improve video quality [25]. Wang et al. propose a social-aware video pre-fetching method based on the distributed online learning for differential privacy by investigation of user preference and social interactions [26]. However, the above methods do not consider the mobility of mobile users and neglect the comprehensive measurement of social relationship and mobile behaviors, which can ensure the performance of video delivery—with some difficulty. Therefore, an efficient method of video delivery should be able to comprehensively measure the social relationship and mobility variation of mobile users to ensure user QoE and QoS of video systems by investigation of user interaction and mobile behaviors.

In this paper, we propose a novel geo-social-aware video edge delivery strategy based on modeling of the social-geographical dynamic in an urban area (GSVD). GSVD investigates social closeness, geographical distance, and video delivery quality to formulate the selection strategy of video providers in order to promote video delivery performance and user QoE. GSVD combines the interactive and basic social relationship for the closeness of the social relationship between mobile users: (1) The frequency of video sharing behaviors and social communication efficiency between users are used to estimate the closeness of interactive social relationship; (2) The estimation of basic social relationship relies on the number of common one-hop social neighbors and the efficiency of a social sub-network consisting of one-hop social neighbors of users. GSVD employs a coding expression method of grid-based geographical location and the calculation method of coding-based geographical distance and formulates an on-demand updating method of geographical location. GSVD further designs a measurement of video delivery quality and a strategy of video delivery adapting to social-geographical dynamic. Simulation results show how GSVD achieves much better performance results in comparison with other state of the art solutions.

## 2. Related Work

Some researchers focus on promoting video delivery performance in video systems with large-scale deployment. Li et al. propose an optimization method of video delivery throughput of a large-scale video-on-demand (VoD) system by investigating the variation of download speed of users based on a dataset of 20 million video download speed measurements [27]. Video quality is an influencing factor for video download speed and determines the intentions of the user requesting the videos, which becomes a limited factor for the speed increases. The video delivery throughput based on the linear regression model is modeled and the potential performance of edge caching and hybrid CDN-P2P is evaluated. However, the conclusion that video download speed is the decisive factor for video request may be partial and may also be suitable for video sharing. Choi et al. proposed a video delivery strategy for dynamic streaming services in playback-delay-constrained wireless caching networks, which maximizes video quality for every unit time [28]. The users make delay-constrained decisions in terms of caching nodes for video delivery, video quality, and quantity of received video chunks; The dynamic decision of video quality and chunk

amounts is described as the Markov decision process and the framework of Lyapunov optimization is used to model the caching node decision. The proposed method considers the delivery performance of videos of caching nodes and describes the dynamic process of video quality decision using the Markov decision process, but the method neglects the user decision of video fetching caused by social influence and the performance jitter of video delivery caused by the mobility of mobile users. The authors propose a cooperative video delivery strategy in wireless networks [29]. By monitoring and estimating the real-time variation in movement behaviors and communication quality of one-hop neighbors of video downloaders, mobility stability of one-hop neighbors is measured and the communication quality of one-hop neighbors is predicted. The cooperative neighbors selection algorithm is designed in terms of mobility stability and communication quality, which speeds up the fetching and dissemination of the videos. The proposed method considers the mobility and communication quality of nodes to ensure the video delivery performance, but the social relationship between the nodes is neglected and the mobility jitter brings a severe negative influence for the video delivery performance. Xiang et al. propose a cross-layer optimization method of video delivery in two-hop relaying networks by supplying the video data for multiple users in a base station with the help of relays [30]. The caching and delivery control schemes are designed in order to minimize the overall video delivery time. An optimization problem of offline caching and delivery is formulated, which exhibits hidden quasi-convexity and convexity. An online video delivery control in a stochastic dynamic programming framework is formulated and a low-complexity online video delivery algorithm is designed. The optimization problem of caching and delivery time does not consider the social influence and mobility of supply users, so that the proposed method difficultly is suitable for social-based video sharing in mobile network.

Some researchers focus on social-based video spread to optimize video distribution and resource allocation. Roy et al. design a transfer learning framework of sudden popularity bursts in online social video streaming [31]. A spread level model of videos in social networks by transfer learning topics in social streams is designed, which promotes the prediction accuracy of video popularity. The conclusion that social context is the main factor of the sudden rise of video popularity is revealed. The main factor for the sudden rise of video popularity is revealed, but the interaction between video interest and social influence are not discussed further. Xu et al. propose a forecast algorithm of video popularity in social networks, which ensures the accuracy and timeliness of video popularity prediction [32]. The popularity prediction investigates the variation and evolution of video propagation patterns in social networks instead of a training phase or prior knowledge. The prediction of the popularity of video spread during a short-term period follows the sublinear and has an explicit bound when the number of video reaches a threshold value. However, the proposed method does not consider the interactive influence between video content and social context for video popularity. Yang et al. make use of the incremental marginal gain to formulate the maximization problem of video spread where the lower and upper bounds of video spread maximization of formulated problem are constructed [33]. An algorithm of sandwich-based marginal increment and an algorithm of video spread maximization are designed, respectively, which guarantees the data-dependent factor and influences the ranking and adjustment of the video spread. However, there are many influence factors of video spread, so that the estimation of the lower and upper bounds of video spread is inaccurate. Niu et al. construct a multiple-source-driven video diffusion model based on the collection and analysis of substantial video diffusion traces [34]. The latency of video propagation along social links is investigated and the single-source activation latency is defined, where the single-source activation latency follows the exponential mixture model. A multi-sources asynchronous diffusion model is constructed, which describes the exponential decreases of activation probability with increasing time. The proposed method reveals the propagation process of videos in social network from single-source to multi-sources, but other influence factors (e.g., the interaction between video content and social relationship) are considered.

Some researchers focus on social-aware video delivery strategies to promote user QoE and the transmission performance of video data. Fan et al. propose a prediction method of social-aware video delivery for the problem of watching decision prediction by content awareness based on capturing the intrinsic relationship among users and videos [35]. The measurement methods of five factors (active degree of users, social tier between users, similarity between videos, similarity between user interest and video content, and video popularity) are designed, which are used to construct the prediction model of video delivery. The combined prediction algorithm of video delivery is designed. The proposed method considers five factors for social influence, video interest and content similarity, but the mobility of the mobile nodes is not considered, which results in the performance jitter of video delivery. The authors propose a social-aware D2D video delivery method in 5G ultra-dense network by measurement of mobility similarity [36]. A social state transition model of user movement is constructed by using encounter duration and shared video length to define the state transition condition. A cluster algorithm of encounter events is proposed in terms of similarity between encounter events, so that the patterns of encounter events with common characteristics is extracted. The cluster-based patterns of encounter events are further refined and are used to generate the refined patterns of encounter events. A sample-efficiency rapid recognition algorithm of encounter pattern is designed, which achieves fast heuristic recognition of encounter pattern. The proposed method only considers the movement encountered in a social relationship and does not consider the social influence and sharing habit, so the inadequate measurement of social influence and video sharing results in the low availability of the proposed method in complex scenarios. Wang et al. review challenges, approaches, and directions of social-aware video delivery [37]. The challenges in social-aware video delivery is present and a principal framework for social-aware video delivery is designed. The unique characteristics of social-aware video access and social content propagation are analyzed and formulated.

### 3. GSVD Overview

Figure 1 illustrates the design of GSVD architecture which includes *social awareness*, *location awareness*, *measurement of video delivery quality*, and *video delivery*. The video systems make use of social networks to implement the fast dissemination of information and data of videos; after the users fetch the information of videos, the video delivery becomes the key factor for the quality of experience (QoE) of users. The near geographical distance and good communication quality are key factors for the performance of video delivery.

(1) *Social Awareness*: Estimation of the interaction behaviors for video sharing can show the closeness of social communications between users by investigating the interactive frequency and content; the estimation of a basic social relationship also shows the common social environment and social communication efficiency between users; the adaptive management for the dynamics of social distance relies on the real-time capture of variation of social distance to show the connectivity of users in social networks.

(2) *Location Awareness*: The location expression based on grid partition for the limited urban area can support the explicit estimation of geographical distance and the adaptive management for dynamic geographical location. The estimation of geographical distance also shows the efficiency of video delivery between users; The adaptive management for the dynamic of geographical distance relies on the periodical capture of variation of geographical location to support the selection of video providers.

(3) *measurement of video delivery quality*: The estimation of transmission time of video data shows the communication quality of transmission paths of video data. The estimation of consistency of video playback shows the QoE and the quality of video delivery in the aspect of viewers.

(4) *Video delivery*: After the estimation of candidate providers in terms of delivery quality, social relationship and geographical distance, the video requesters need to make use of the social links to search for and contact the video providers, to monitor the delivery quality, and make the decision for the switchover of providers in terms of location variation.

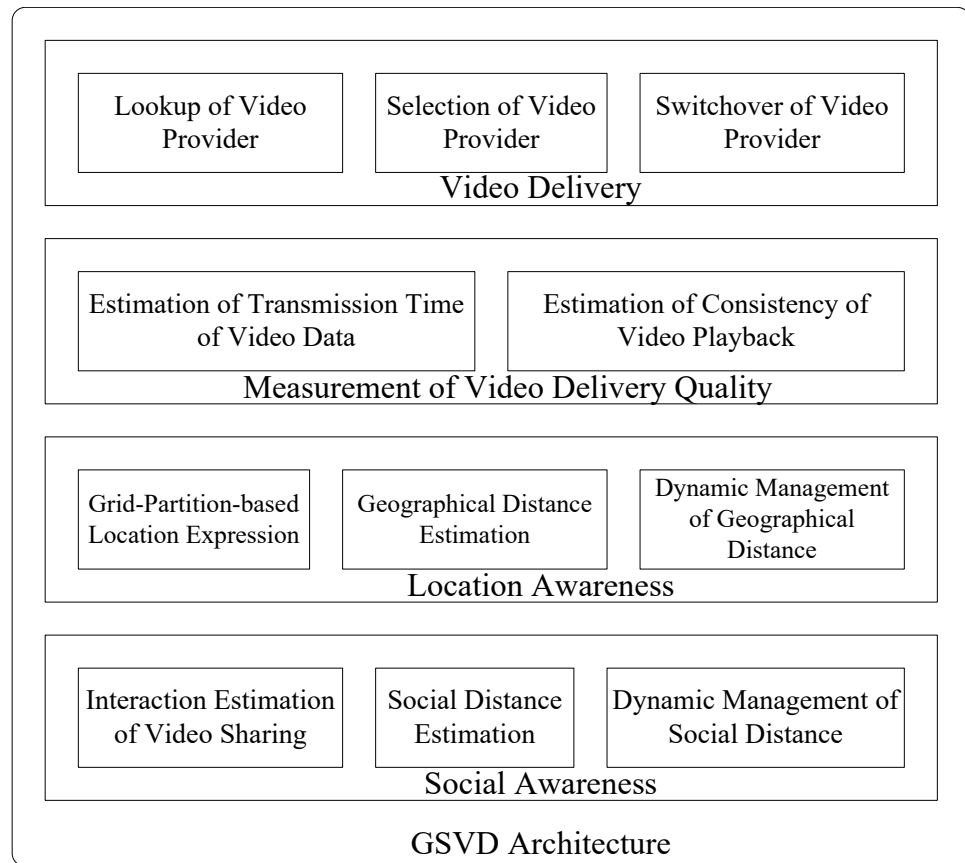


Figure 1. GSVD architecture.

#### 4. GSVD Detailed Design

##### 4.1. Measurement of the Social Relationship

A close social relationship promotes video sharing between users. For instance, a user  $u_i$  can always obtain the desired video resources from the good friend  $u_j$  of  $u_i$ ;  $u_i$  always pushes the watched videos to  $u_i$ 's friends. The video sharing without the participation of video servers promotes the scalability of video systems and the range and speed of video dissemination. The frequent sharing of videos is a characteristic of a close social relationship between users. If  $u_i$  sends a video  $v_k$  to  $u_j$  and  $u_j$  responds the request of  $u_i$  and transmits data of  $v_k$  to  $u_i$ , the event of video sharing between  $u_i$  and  $u_j$  can be recorded as  $e = (eid, uid_r, uid_p, vid, flag)$ .  $eid$  is the ID of event;  $uid_r$  is the ID of requester;  $uid_p$  is the ID of provider;  $vid$  is the ID of shared video;  $flag$  is the ID of shared way ("pull" or "push") where "pull" is 1 and "push" is 2. For instance,  $e_{ij}$  is the five-tuples and  $e_{ij} = (1, u_i, u_j, v_k, 1)$ . The events of sharing of all videos form a set  $ES = (e_1, e_2, \dots, e_n)$ .

The important information in the event of video sharing is recorded: (1) all users (requesters and providers) that watch any video; (2) all interaction behaviors between all users that watch any video. For instance, the number  $IF_{ij}$  of interaction behaviors ("pull" or "push") between  $u_i$  and  $u_j$  can be extracted from  $ES$ . The interaction closeness between  $u_i$  and  $u_j$  can be defined as:

$$IC_{ij}^w = \frac{1}{d_{ij}} \text{MIN} \left[ \frac{IF_{ij}}{IF_i}, \frac{IF_{ij}}{IF_j} \right] \tag{1}$$

where  $IF_i$  is the total number of interaction behaviors between  $u_i$  and other users;  $IF_j$  are the total number of interaction behaviors between  $u_j$  and other users.  $\frac{IF_{ij}}{IF_i}$  and  $\frac{IF_{ij}}{IF_j}$  are the partial closeness of interaction behaviors relative to  $u_i$  and  $u_j$ , respectively. The interaction closeness between  $u_i$  and  $u_j$  is the minimum value between  $\frac{IF_{ij}}{IF_i}$  and  $\frac{IF_{ij}}{IF_j}$ . Further, we add

a weight value  $\frac{1}{d_{ij}}$  for  $IC_{ij}$  where  $d_{ij}$  is the shortest distance between  $u_i$  and  $u_j$  in social networks and  $d_{ij}$  denotes the communication efficiency in social networks.

Moreover, the basic social relationship between  $u_i$  and  $u_j$  should also be investigated. The users have a complex social environment, e.g., they could be relatives and colleagues in the real world. If the two users  $u_i$  and  $u_j$  have many common friends, the basic social relationship between  $u_i$  and  $u_j$  is strong, which can support the high-frequency interaction between  $u_i$  and  $u_j$ ; Otherwise, if  $u_i$  and  $u_j$  have less common friends, the basic social relationship between  $u_i$  and  $u_j$  is weak and the interaction between  $u_i$  and  $u_j$  may be random. Let  $NF_i$  and  $NF_j$  be the number of one-hop social neighbors of  $u_i$  and  $u_j$ , respectively, and  $NF_i$  and  $NF_j$  can also be considered as the degree of  $u_i$  and  $u_j$ , respectively. The basic social relationship between  $u_i$  and  $u_j$  can be defined as:

$$BR_{ij}^{\omega} = \frac{CN_{ij}^2}{d_{ij} \times NF_i \times NF_j} \quad (2)$$

where  $CN_{ij}$  is the number of common one-hop social neighbors between  $u_i$  and  $u_j$ ;  $\frac{CN_{ij}}{NF_i}$  is the ratio between common one-hop social neighbors between  $u_i$  and  $u_j$  and one-hop social neighbors of  $u_i$ ;  $\frac{CN_{ij}}{NF_j}$  is the ratio between common one-hop social neighbors between  $u_i$  and  $u_j$  and one-hop social neighbors of  $u_j$ . We also add a weight value  $\frac{1}{d_{ij}}$  for  $BR_{ij}$ .  $\frac{CN_{ij}}{d_{ij} \times NF_i \times NF_j}$  denotes the efficiency of a social sub-network consisting of one-hop social neighbors of  $u_i$  and  $u_j$ . Therefore,  $BR_{ij}$  is not only the basic social relationship between  $u_i$  and  $u_j$ , but also denotes the capacity of the video distribution of a social sub-network consisting of one-hop social neighbors of  $u_i$  and  $u_j$ . The closeness of the social relationship between  $u_i$  and  $u_j$  can be defined as:

$$CR_{ij} = IC_{ij}^{\omega} \times BR_{ij}^{\omega} \quad (3)$$

The shortest social distance between  $u_i$  and  $u_j$  is a very important influence factor in  $CR_{ij}$ , which determines the cost and efficiency of social communications between  $u_i$  and  $u_j$ . The low value of the shortest social distance can reduce the number of relay users of social communication between  $u_i$  and  $u_j$ , which speeds up the interaction of video information. The larger/smaller the shortest social distance between  $u_i$  and  $u_j$  is, the lower/higher the closeness of the social relationship between  $u_i$  and  $u_j$  is. However, the shortest social path between  $u_i$  and  $u_j$  is various. For instance, if  $u_i$  and  $u_j$  do not have direct social link and need to make use of social links of other users to implement social communications; once  $u_i$  and  $u_j$  build social link after video interaction, the length of shortest social path between  $u_i$  and  $u_j$  become one hop from multiple hop. The cost/efficiency of social communications between  $u_i$  and  $u_j$  is reduced/promoted. On the other hand, if  $u_i$  and  $u_j$  have one-hop social relationship at  $t_i$  and remove their one-hop social relationship at  $t_j$ , the multiple-hop social links between  $u_i$  and  $u_j$  increases the cost of social communications. However, the users need to maintain the state of social links to deal with the dynamic of social links. The real-time maintenance of social links consumes the large amount of bandwidth resources. Therefore, the periodical maintenance of social links reduce the bandwidth cost of state messages. Let  $TL_i$  be the maintenance period time of social links of  $u_i$ ; Let  $NL_i$  be the number of changed one-hop social links of  $u_i$  during the period time  $TL_i$ . The variation rate of one-hop social links of  $u_i$  can be defined as:

$$LR_i = \frac{NL_i}{TL_i} \quad (4)$$

The higher the value of  $LR_i$  is, the shorter the period time of updating one-hop social links of  $u_i$  is. The short period time adapts to the fast change of one-hop social links of users. If the value of  $LR_i$  is high, the long period time reduces the cost of updating one-hop social links of  $u_i$ . The dynamic update period time of  $u_i$  can be defined as:

$$UT_i = \frac{TL_i}{LR_i} = \frac{TL_i^2}{NL_i} \tag{5}$$

The users can dynamically change the update period time with a low message cost and obtain the accurate state of social links with other users in terms of the above equation.

#### 4.2. Measurement of the Geographical Location

The geographical location of users is also an important influence factor for the performance of video delivery. The dynamic of geographical location of users leads to the variation of transmission path of video data. For instance, a user  $u_i$  has one-hop geographical distance with another user  $u_j$  at  $t_i$ ;  $u_i$  has multiple hop geographical distance with  $u_j$  at  $t_j$ . The transmission performance of video data  $u_i$  and  $u_j$  may be influenced by the variation of the geographical distance between  $u_i$  and  $u_j$ .

An urban area has a limited boundary, and the range of an urban area is also limited. An urban area can be divided and coded, so the coded subarea can express the geographical location. As Figure 2 shows, an urban area is divided into  $5 \times 5$  grids (red dashed line) and each grid has a unique number to express the a well-bounded subarea. The user A has the explicit code  $loc_{12}^A$  of geographical location. The grid partition strategy has a large influence on the expression of the geographical location of users. The larger the range of the divided subarea is, the lower the accuracy of the expression of the geographical location is; Otherwise, the smaller the range of the divided subarea is, the higher the frequency of updating the geographical location is. The range of the divided subarea can be equal to the coverage area of the access point (AP) and the grid partition strategy can employ the deployment method of cellular APs. In terms of the Euclidean distance, the code-based geographical distance between the two users  $u_i$  and  $u_j$  can be defined as:

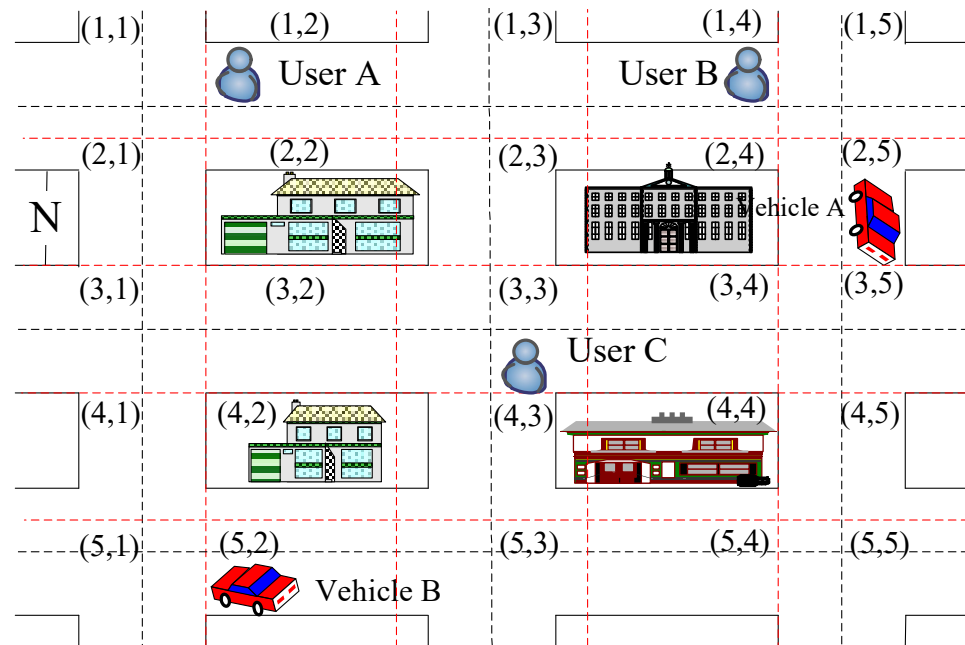


Figure 2. Grid-based partition in the urban area.

$$D_{ij} = \sqrt{(x_i - x_j)^2 + (y_i - y_j)^2} \quad (6)$$

where  $x_i, y_i, x_j$  and  $y_j$  are the horizontal and vertical coordinates of  $u_i$  and  $u_j$ , respectively. For instance, the codes of geographical location of  $u_i$  and  $u_j$  are  $loc_{12}^i$  and  $loc_{14}^j$ , so  $x_i = 1, y_i = 2, x_j = 1, y_j = 4$  and  $D_{ij} = 2$ .  $D_{ij}$  is not the real geographical distance between  $u_i$  and  $u_j$  and is code-based geographical distance. If the grid partition strategy employs the deployment method of cellular APs, the diameter  $R$  of cellular APs is a code-based unit distance and the real geographical distance between  $u_i$  and  $u_j$  is  $D_{ij} \times R = 2R$ . The urban area is divided into  $m \times n$  subarea where  $m$  and  $n$  are the codes of row and column of each subarea, respectively. The code of each subarea is in the range  $[(1, 1), (m, n)]$ ; the shortest and largest geographical distance are  $[0, R\sqrt{(m-1)^2 + (n-1)^2}]$ , respectively (when two users are located at the same subarea, the shortest geographical distance between them is 0). The normalization result of real geographical distance between  $u_i$  and  $u_j$  is defined as:

$$ND_{ij} = \frac{D_{ij} - D_{\min}}{D_{\max} - D_{\min}} = \frac{D_{ij}}{\sqrt{(m-1)^2 + (n-1)^2}} \quad (7)$$

The users make use of the mobile devices to obtain video data via the Internet, so the geographical location of the users is a dynamical change. The variation frequency of geographical location users is higher than that of social distance, so that any user does not maintain the geographical location of other users in real time due to the large scale and high frequency of maintenance. Because the users make use of the social links to disseminate the information and data of videos, the users only maintain the geographical location of one-hop social neighbors for the maintenance scale. For the maintenance frequency, different from the periodical maintenance of social links, we employ an on-demand update strategy of geographical location of one-hop social neighbors. When a user  $u_i$  requests a video  $v_k$  from  $u_j$  or pushes  $v_k$  for another user  $u_j$ ,  $u_i$  sends the multicast messages containing the request of updating the geographical location to one-hop social neighbors of  $u_i$ .  $u_i$  updates the geographical location to one-hop social neighbors after receiving the response messages.  $u_i$  makes use of the updated geographical location to calculate the geographical distance with one-hop social neighbors. The calculated geographical distance can be used to select video providers or relay users in the process of video lookup.

#### 4.3. Measurement of Video Delivery Quality

There is a close relationship between video quality and user QoE. The continuity of video playback is very important for the user QoE. The continuity of video playback relies on the communication quality in the transmission path of video data. The transmission time and loss rate of video data are measurement parameters of the communication quality. If the transmission time of the video data is close to the length of the videos, the number of playback interrupt maintains low levels; if the loss rate of video data is close to 0, the number of playback interrupt also maintains low levels. The high quality of video delivery denotes the high quality of services of video providers. For instance, a user  $u_i$  requests a video  $v_k$  and fetches video data from  $u_j$ . Let  $VL_k$  be the length of  $v_k$  and the service level about transmission time of  $u_j$  can be defined as:

$$QT_j = \frac{L_k}{\overline{TL_k^j}}, QT_j \in (0, 1] \quad (8)$$

where  $\overline{TL_k^j}$  is the average value of transmission time of  $u_j$  for the  $u_j$  of all requesters regarding  $v_k$  and is defined as:

$$\overline{TL_k^j} = \frac{\sum_{c=1}^{SN_j^k} TL_c}{SN_j^k} \quad (9)$$

where  $SN_j^k$  is the number of requesters served by  $u_j$ ;  $TL_c$  is the transmission time of  $c^{th}$  service of  $u_j$ . The value of  $\overline{TL_k^j}$  is in the range  $[L_k, +\infty)$  and  $QT_j \in (0, 1]$ . On the other hand, let  $\overline{l_{f_k}^j}$  be the average value of loss times of video data of  $u_j$  and the value of  $\overline{l_{f_k}^j}$  is defined as:

$$\overline{l_{f_k}^j} = \frac{\sum_{c=1}^{SN_j^k} l_{f_c}}{SN_j^k} \quad (10)$$

where  $l_{f_c}$  is the loss times of  $c^{th}$  service of  $u_j$ . The service level about loss rate of video data of  $u_j$  can be defined as:

$$QL_j = \frac{1}{\overline{l_{f_k}^j} + 1}, QL_j \in (0, 1] \quad (11)$$

The value of  $\overline{l_{f_k}^j}$  is in the range  $[0, +\infty)$  and  $QL_j \in (0, 1]$ . The smaller the value of  $\overline{l_{f_k}^j}$  is, the larger the value of  $QL_j$  is.  $QT_j$  and  $QL_j$  are the important parameters for the service level of  $u_j$ . Therefore, the service level  $u_j$  can be defined as:

$$Q_j = QT_j \times QL_j \quad (12)$$

The values of  $QT_j$  and  $QL_j$  maintain high levels, so the continuity of video playback of requesters served by  $u_j$  is high. There is a close relation between transmission time and data loss. If the loss rate of video data is high, the retransmission of video data leads to the increase of transmission time of video delivery.  $QT_j$  and  $QL_j$  have the same trend of variation.

#### 4.4. Video Delivery Strategy

Video delivery includes video lookup and data transmission. Video lookup means that the requesters find and connect with the providers where to store the needed videos in the networks. For instance, when a user  $u_i$  wants to fetch a video  $v_k$ ,  $u_i$  can obtain the set of candidate providers which store  $v_k$  according to the event set of video sharing and needs to select the providers with high delivery capacity from the large number of candidate providers. The delivery capacity of video should have a short lookup delay of providers and a short transmission delay of video data. The requesters need to make use of the social links between users to forward the request message of  $v_k$  in the process of social-based video lookup. Therefore,  $u_i$  selects the provider that has a strong social relationship with  $u_i$  as much as possible. Further, the interaction of video sharing promotes the closeness of social relationship between  $u_i$  and the selected provider. On the other hand, the stability and efficiency of video data transmission relies on the geographical distance between  $u_i$  and the selected provider. The close geographical distance can ensure the stability and efficiency of video data transmission with less relay nodes. Moreover, the selected provider

should also have high service quality.  $u_i$  needs to calculate the delivery capacity of each candidate providers according to the following equation.

$$QD_j = \frac{CR_{ij} \times Q_j}{ND_{ij}} \quad (13)$$

$CR_{ij}$  and  $Q_j$  is the increasing function; the larger the values of  $CR_{ij}$  and  $Q_j$  are, the larger the value of  $QD_j$  is.  $\frac{1}{ND_{ij}}$  denotes the efficiency of geographical communication between  $u_i$  and provider  $u_j$  and  $ND_{ij}$  is the decrease function; The less the value of  $ND_{ij}$  is, the larger the value of  $QD_j$ .  $u_i$  should select the provider that has the largest value of  $QD_j$ .

The video lookup relies on the forwarding of request messages. The users in social networks not only store the event set of video sharing to be aware of candidate providers of videos, but also to maintain the information of one-hop social neighbors to support the forwarding of request messages. For instance,  $u_i$  needs to maintain a set  $US_i = (un_1, un_2, \dots, un_m)$  of one-hop social neighbors. Any item  $un_h$  in  $US_i$  is defined as  $un_h = (uid, VL, GL, ut)$  where  $uid$  is the ID of the one-hop social neighbor;  $VL$  is the list of videos stored by the one-hop social neighbor;  $GL$  is the code of the geographical area;  $ut$  is the timestamp of updating the state of the one-hop social neighbor.

If  $u_i$  wants to fetch a video  $v_k$ ,  $u_i$  searches for the items in  $US_i$  which store  $v_k$ . If  $US_i$  has a subset  $SUS_i$  whose items store  $v_k$ ,  $u_i$  sends the request messages to the items in  $SUS_i$ . After the items in  $SUS_i$  receive the request messages of  $u_i$ , they return the response messages containing the current code of geographical location and confirmation mark  $flag$  to  $u_i$ . The values of  $flag$  are 0 (the user does not store  $v_k$ ) and 1 (the user stores  $v_k$ ):

(1) If all items in  $SUS_i$  do not store  $v_k$  due to the dynamic variation of local storage space,  $u_i$  is aware of the request results in terms of  $flag$  in the return messages and all items in  $SUS_i$  broadcast the request message of  $u_i$  to their one-hop social neighbors. Further,  $u_i$  broadcast the request messages to items in  $US_i - SUS_i$  (the difference set between  $US_i$  and  $SUS_i$ ). The request messages of  $u_i$  are disseminated with the flooding in the whole social networks. After the relay users receive the return message with  $flag = 1$  of one-hop social neighbors, they broadcast the messages containing the termination of the flooding to their one-hop social neighbors and return the response messages to  $u_i$ .  $u_i$  receives the return messages containing the response user ID and codes of geographical location.  $u_i$  selects and connects with the provider that has the largest value according to Equation (13) from the items in  $SUS_a$  and receives data of  $v_k$  from the selected provider.

(2) If there are items in  $SUS_i$  that store  $v_k$ , the items in  $SUS_i$  return the messages with  $flag = 1$ . After  $u_i$  receives the return messages,  $u_i$  sends the messages containing the termination of the flooding to the items in  $SUS_i$ .  $u_i$  selects and connect with the provider that has the largest value according to Equation (13) from the items in  $SUS_i$ .  $u_i$  receives data of  $v_k$  from the selected provider.

The algorithm of provider selection is described in Algorithm 1. The mobility of the mobile users leads to the dynamic variation of transmission paths video data, which brings a severely negative influence for the transmission performance of video data (e.g., a high loss rate of data).  $u_i$  needs to keep the contact with the candidate providers with a large value of  $QD$ . Once the communication quality of the data transmission path between the provider is less than the threshold value of QoE of  $u_i$  (the loss rate of data is higher than the threshold value  $P_i$  of QoE of  $u_i$ ),  $u_i$  disconnects with the provider and connects with the new provider with the maximum value of  $QD$  according to Equation (13).

**Algorithm 1** Video Provider Selection

---

```

1:  $T_i$  is maximum value of startup delay of  $u_i$ ;
2:  $CD_i$  is set of candidate providers;
3:  $t$  is timer and  $t = 0$ ;
4: for ( $j = 0$ ;  $j < |US_i|$ ;  $j++$ )
5:   for ( $h = 0$ ;  $h < |US_i[j].VL|$ ;  $h++$ )
6:     if  $US_i[j].VL[h]$  is  $v_k$ 
7:        $US_i[j]$  is added into  $SUS_i$ ;
8:     end if
9:   end for
10: end for
11: sends request messages to items in  $SUS_i$ ;
12: receives return messages from items in  $SUS_i$ ;
13: if items in  $SUS_i$  do not have  $v_k$ 
14:   requires flooding by broadcasting messages to  $US_i$ ;
15: while  $T_i = t$ 
16:   if receives return message with  $flag = 1$ 
17:     candidate providers are added into  $CD_i$ ;
18:   end if
19:    $t++$ ;
20: end while
21: end if
22: calculates  $QD$  of items in  $SUS_i$  and  $CD_i$ ;
23: connects with provider with maximum value of  $QD$ ;
24: receives video data from selected provider;

```

---

**5. Testing and Results Analysis***5.1. Testing Topology and Scenarios*

We compare the performance of the proposed solution GSVD with that of the two state of the art solutions DMSEM [36] and SECS [38], which are deployed in a mobile network environment by making use of the Network Simulator 3 (NS-3). The simulation time is set to 500 s. A total of 500 mobile nodes are uniformly deployed in a square scenario in a  $4000 \times 4000 \text{ m}^2$  area and maintain the random movement behaviors during the whole simulation time. Initially, the mobile nodes have the position coordinates of the beginning and the ending. They are allocated randomly at a constant speed and move along the path consisting of the beginning and the ending position. When the mobile nodes arrive at the appointed ending position, they have 0 s stay time and are randomly reassigned a new destination position and a movement speed. The mobile nodes move immediately to the new target and follow the new destination position using the new allocated speed. The velocity of the mobile nodes is in the range [1, 30] m/s.

There are 40 videos that are requested by the mobile nodes. The popularity of all videos follows the Zipf distribution [39]. The probability of requesting the  $n^{\text{th}}$  popular video is defined as [40]:

$$P(n) = \frac{\sum_{40}^i i^\rho}{r^\rho} \quad (14)$$

The mobile nodes follow the request probabilities to request videos and follow the Poisson distribution start video request. When the mobile nodes request a video, the playback time is randomly set and is allocated to the mobile nodes. After the mobile nodes finish the playback according to the allocated playback time, they continue to request a new video according to the request probabilities. The length and size of every video is 100 s and 25 MB, respectively. The playback bitrate of all videos is 2000 kbps. Every mobile node can store 10 videos in the local buffer. The number of source nodes that store the initial video data is set to 10, which means that 40 nodes provide the initial data of 40 videos. We generate 20,000 log entries that are considered as a historical playback trace library to support the social relationship measurement of GSVD and interest-based user clustering of SECS; we also build a historical movement trace library to support the mobility-adapted video quality estimation of GSVD and the extraction of encountered patterns of DMSEM. The simulation scenarios uniformly deploy 64 base stations that are used as the access points (APs) to transmit and forward data. The settings of physical and MAC layer and modulation schemes of the network units follow the 5G industrial standardization. The MAC protocol employs the 802.11p and the upper bound of the data rate is set to 27 Mbps. The maximum communication range is 250 m and the MAC channel delay is 250 ms. The propagation loss model employs the Friis Propagation Loss Model (FPLM) in NS3 [41] in order to eliminate the performance degraded by random shadowing effects for the unstructured clear path between receivers and transmitters. The FPLM effectively erases the random effects caused by shadowing for the simulation results. The D2D settings of the 5G network follows the settings in the popular studies [42].

### 5.2. Performance Evaluation

We compare the performance of GSVD with DMSEM and SECS in terms of the startup delay (SD), average data transmission delay (ADTD), packet loss rate (PLR), average freeze time (AFT), and peak signal-to-noise ratio (PSNR), respectively.

Startup delay (SD): Let  $t_{si}$  be the time that a request node  $n_i$  sends a request message to the video supply node  $n_j$ ; Let  $t_{ri}$  be the time that  $n_i$  receives the first video data sent by  $n_j$ .  $t_{ri} - t_{si}$  is defined as the startup delay of  $n_i$ .

The average SD values for every 5 s are shown in Figure 3 according to the equation  $\frac{\sum_{i=1}^n SD_i}{n}$  where  $n$  is the number of nodes which finish startup and  $SD_i$  is  $i^{th}$  the startup delay. As Figure 3 shows, the three curves corresponding to the three solutions have the process of a slow fall after a fast rise with the slight fluctuation. The blue curve of GSVD first experiences a slow rise from  $t = 110$  s to  $t = 240$  s after a fast rise from  $t = 0$  s to  $t = 100$  s and have a slow fall from  $t = 250$  s to  $t = 500$  s. The red curve of DMSEM has a fast rise from  $t = 0$  s to  $t = 260$  s and experiences a slow fall from  $t = 270$  s to  $t = 500$  s. The orange curve of SECS has a fast rise from  $t = 0$  s to  $t = 250$  s and keeps a slow fall trend from  $t = 260$  s to  $t = 500$  s. The SD values of GSVD is partially larger than those of DMSEM and SECS from  $t = 0$  s to  $t = 150$  s, but the SD values of GSVD are less than those of  $t = 160$  s to  $t = 500$  s. The peak value of blue curve corresponding to GSVD is less than that of DMSEM and SECS. SECS has the largest SD peak value among the three solutions.

The average SD values during the whole simulation time with the different speed range of nodes are shown in Figure 4. As Figure 4 shows, the average SD values corresponding to the three solutions have the trend of slow rise with an increasing speed range of nodes. The blue bars of GSVD experience the continuous rise and have a fast increase from the speed range [5, 10] to [15, 20] and from the speed range [15, 20] to [25, 30]. The red bars of DMSEM also have a continuous rise and a fast increase from the speed range [5, 10] to [15, 20] and from the speed range [15, 20] to [20, 25]. The orange bars of SECS show the continuous rise and also a the fast increase from the speed range [5, 10] to [15, 20] and from the speed range [15, 20] to [20, 25]. The SD values of GSVD are less than those of DMSEM and SECS, and the SD values of SECS are larger than those of GSVD and DMSEM.

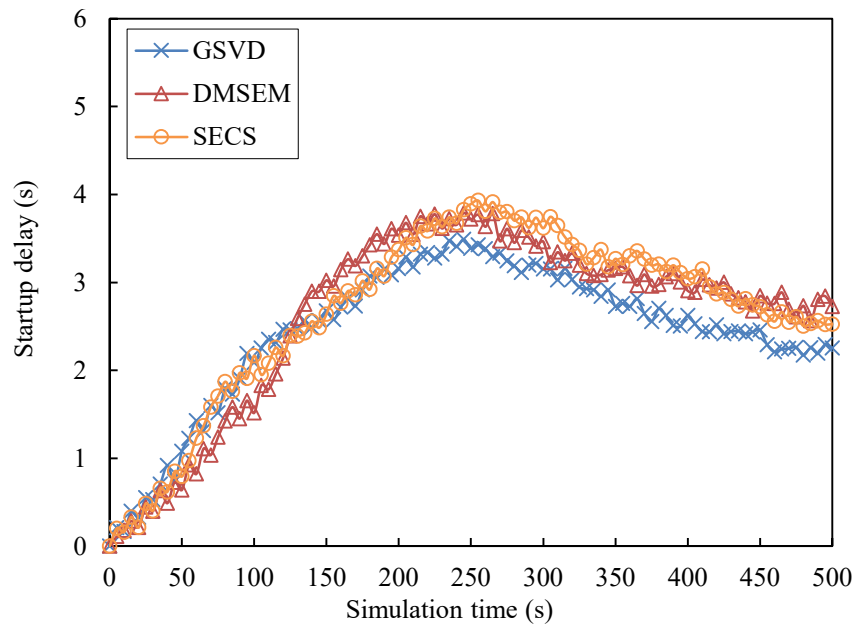


Figure 3. Startup delay against the simulation time.

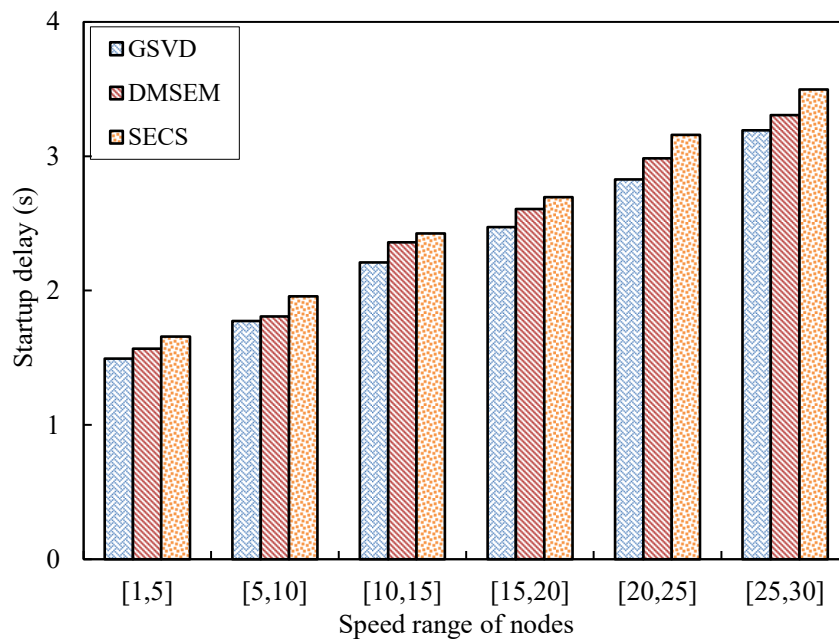


Figure 4. Startup delay against the various speed ranges of the nodes.

The factors that bring the influence for the SD values include supplier lookup delay, capacities of handling requests for the supplier, and delivery performance of the request messages and first video data. GSVD investigates the relationship of sociability and location between users in terms of video sharing behaviors and grid-based location awareness. GSVD enables the video request nodes that depend on the social paths to search for video supply nodes in terms of the interaction behaviors of video sharing between nodes, which promotes the lookup success rate and reduces the delay of supply node lookup. On the other hand, GSVD tracks the geographical location of mobile nodes, which ensures the near geographical distance between mobile nodes in order to provide high-powered delivery of data. Moreover, GSVD makes use of the transmission time of video data and the consistency of video playback to measure the video delivery quality of nodes, which ensures a low transmission time of the request message and video data. Although the SD values of GSVD quickly increase at the time phasing of intensive request due to the

short-term deficiency of upload bandwidth supply caused by the negligence of redundancy distribution of video copies, the high-efficiency delivery performance of video data achieves the fast spread of video copies, which effectively relieves the unbalance between the supply and demand. Therefore, the SD values of GSVD are less than those of DMSEM and SECS. DMSEM investigates the one-hop D2D pair relationship, compares the encounter duration and shared video length, and defines the encounter events based on the variation rate of the geographical distance between mobile users and encounter duration time. DMSEM makes use of the Fuzzy C-Means to group encounter events into the various clusters according to iterative search and emergence. DMSEM considers the clusters of encounter events as counter patterns of mobile users and depends on the rapid recognition algorithm of encounter behaviors to achieve fast heuristic recognition of encounter events, which supports the high-efficiency video sharing based on one-hop D2D pair. However, DMSEM does not consider video lookup, so the lookup success rate is not ensured, which results in a high delay of video lookup. On the other hand, DMSEM also does not consider the redundancy distribution of video copies, which does not effectively address the problem of imbalance between supply and demand. When a large request of video arrives, the low capacities of the handling request caused by the imbalance between supply and demand results in the increases of the wait delay for the request nodes. Similar to GSVD, DMSEM also relies on the high performance of delivery of request message and video data to speed up the spread of video copies and promote the capacities of the video supply. Moreover, DMSEM relies on one-hop D2D communications to transmit video data, so the probabilities of the one-hop D2D pair bring a negative influence for the startup delay of the request nodes. Therefore, the SD values of DMSEM are higher than those of GSVD. SECS constructs the interest domain of users and clusters the users with common interests into the same groups, which defines the range of video sharing objects between the users. The intragroup video sharing relies on the common interests of users and can obtain a high success rate of video lookup, which reduces the video lookup delay. SECS employs “pull” and “push” modes to spread video between users to achieve a fast increase of the redundancy copies, which effectively promotes the capacities of video supply and reduces the wait delay of the request nodes. However, SECS does not consider the precondition of demand scale, so the imbalance between supply and demand caused by the stampeded request of videos is relieved only for a limited time. On the other hand, although SECS considers the sharing performance for the caching replacement and distribution, SECS does not investigate the relationship and variation of geographical location of video requesters and suppliers. The variation of movement behaviors and speed brings a severely negative influence for the transmission of request message and video data. Therefore, the SD values of SECS are higher than those of GSVD and DMSEM.

**Average data transmission delay (ADTD):** The end-to-end transmission delay of video data is defined as the data transmission delay. The average data transmission delay can be defined as  $\frac{\sum_{i=1}^n dt_i}{n}$  where  $n$  is the number of delay of transmitted data during a time span  $t$  and  $dt$  is the delay of the transmitted data. The ADTD values for every 5 s are shown in Figure 5 and the ADTD values with various speed range of nodes are shown in Figure 6.

As Figure 5 shows, the three curves corresponding to SDMS, OCP, and SECS have a severe jitter process with the increasing simulation time. The blue curve of GSVD keeps lower levels than those of DMSEM and SECS and the ADTD peak value of GSVD is less than those of DMSEM and SECS. The ADTD peak value of DMSEM is lower than that of SECS. SECS has the largest ADTD peak value among the three solutions and the orange curve of SECS has higher levels than those of GSVD and DMSEM.

As Figure 6 shows, the average ADTD values corresponding to the three solutions have the trend of a slow rise with an increasing speed range of nodes. The blue bars of GSVD keep the rise trend and have a fast increase from the speed range [5, 10] to [15, 20] and from the speed range [15, 20] to [25, 30]. The blue bars of GSVD are lower than those of DMSEM and SECS. The red bars of DMSEM have a fast rise, where the red bar of DMSEM is higher than that of SECS at the speed range [1, 5] and the red bar of DMSEM is higher

than that of SECS at the speed range [5, 10]. The red bars of DMSEM are lower than those of SECS from the speed range [15, 20] to [25, 30].

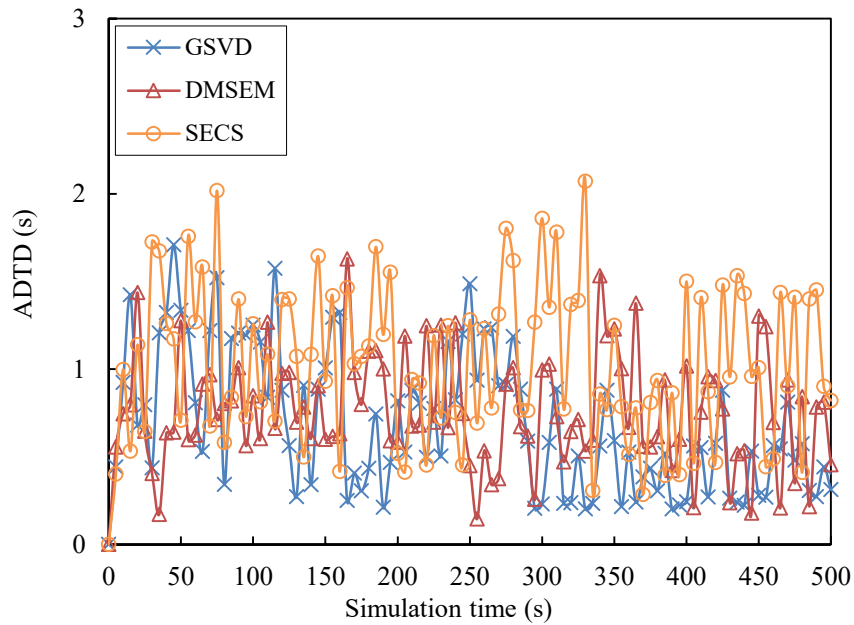


Figure 5. Average data transmission delay against simulation time.

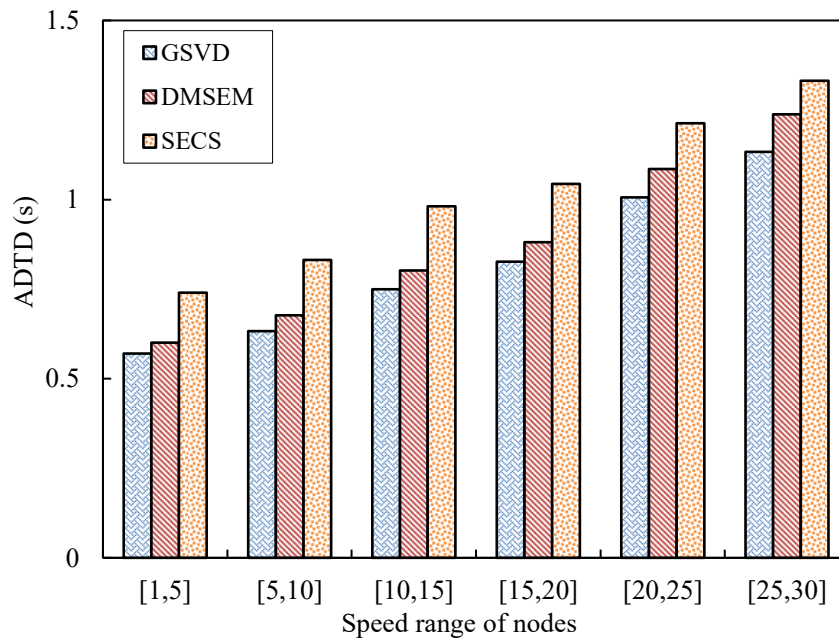


Figure 6. Average data transmission delay against various speed range of nodes.

GSVD divides the urban area into multiple coded grids and makes use of the grid codes to express the geographical location of the mobile nodes. GSVD depends on the code-based geographical location to calculate the geographical distance between the mobile nodes. GSVD investigates the transmission delay and loss rate in the process of video data delivery and constructs the estimation of video delivery quality in order to ensure video delivery performance and user QoE. GSVD designs a strategy of video delivery to allocate the optimal video supply node to calculate the delivery capacity of candidate supply nodes using the calculated social and geographical distance and video delivery quality, which adapts to the social-geographical dynamic to ensure video delivery performance and user QoE. The dynamic mobility of nodes results in the dynamic variation of data transmission

paths; the intensive video request leads to the fast consumption of network bandwidth during a short time period. The dynamic mobility and the intensive request brings a severely negative influence, so that the ADTD values of GSVD keep a fast increase with the increasing levels of intensive request and speed range of nodes. However, the ADTD values of GSVD are less than those of DMSEM and SECS. DMSEM investigates the encounter duration and shared video length to define the encounter events in terms of measurement of the variation rate of the geographical distance between mobile users and the encounter duration time. DMSEM clusters the encounter events in terms of similarities between them to extract the encounter patterns of the mobile nodes. DMSEM relies on the extracted encounter patterns to recognize the encounter behaviors, which supports the high-efficiency video sharing by pairing one-hop D2D communication parties before future encounters. Although DMSEM depends on one-hop D2D communications between mobile nodes to implement high-efficiency data delivery, the mobility of mobile nodes brings a severely negative influence. Once video requesters or suppliers are out of D2D communication range, the video requesters re-search suppliers in order to address the problem of data transmission interruption. Moreover, the huge bandwidth consumption caused by the intensive short-term video request and the signal attenuation caused by the increasing geographical distance also promotes the risk of ADTD rise. SECS focuses on the economic supply of upload bandwidth by clustering the users with common interests and employing “pull” and “push” modes to spread video between the users. Although SECS considers the sharing performance in order to efficiently implement the caching distribution and replacement with low cost, the mobility of mobile nodes related to video data transmission cannot be considered. Therefore, the ADTD values of SECS are influenced with high probabilities, so that SECS has higher ADTD values than those of GSVD and DMSEM.

Packet loss rate (PLR): The ratio between the number of lost video data during a time span  $t$  and the total number of sent video data during  $t$  is defined as the packet loss rate. The PLR values during  $t = 10$  s are shown in Figure 7.

As Figure 7 shows, the three solutions keep the fall trend with the slight fluctuation during the whole simulation time. The blue curve of GSVD has a fast fall trend from  $t = 0$  s to  $t = 180$  s and keeps a slight decrease with the slight fluctuation from  $t = 190$  s to  $t = 500$  s. The PLR curve of GSVD are lower than those of DMSEM and SECS during the most of simulation time. The red curve of DMSEM has a fast fall from  $t = 0$  s to  $t = 110$  s and a slow fall from  $t = 120$  s to  $t = 350$  s and keeps a stable trend from  $t = 360$  s to  $t = 500$  s. The orange curve of SECS has a fast fall from  $t = 0$  s to  $t = 160$  s, experiences a transient stable levels from  $t = 170$  s to  $t = 230$  s and keeps a slight decrease from  $t = 240$  s to  $t = 500$  s. The red curve of SECS is higher than those of GSVD and DMSEM.

As Figure 8 shows, the bars corresponding to the three solutions maintain a rising trend with various speed ranges for the nodes. The blue bars of GSVD have a stable rise with an increasing speed of the nodes and are lower than those of DMSEM and SECS. The red bars of DMSEM have a stable rise for the speed range of the nodes from [1, 5] to [20, 25] and a fast increase at the speed range [25, 30]. The orange bars of SECS maintain a slow increase for the speed range of the nodes from [1, 5] to [5, 10] and have a fast rise from [10, 15] to [25, 30]. The orange bars of SECS are higher than those of GSVD and DMSEM.

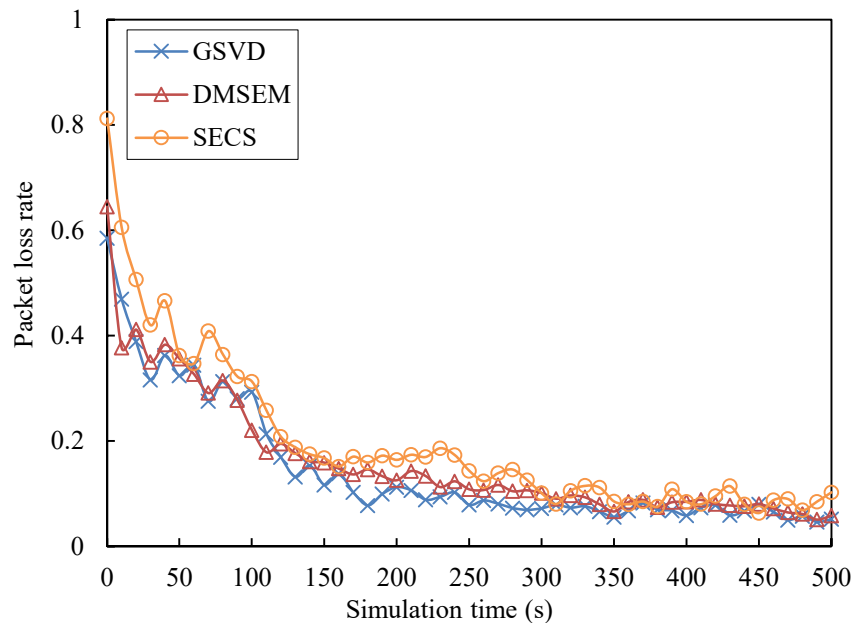


Figure 7. Packet loss rate against the simulation time.

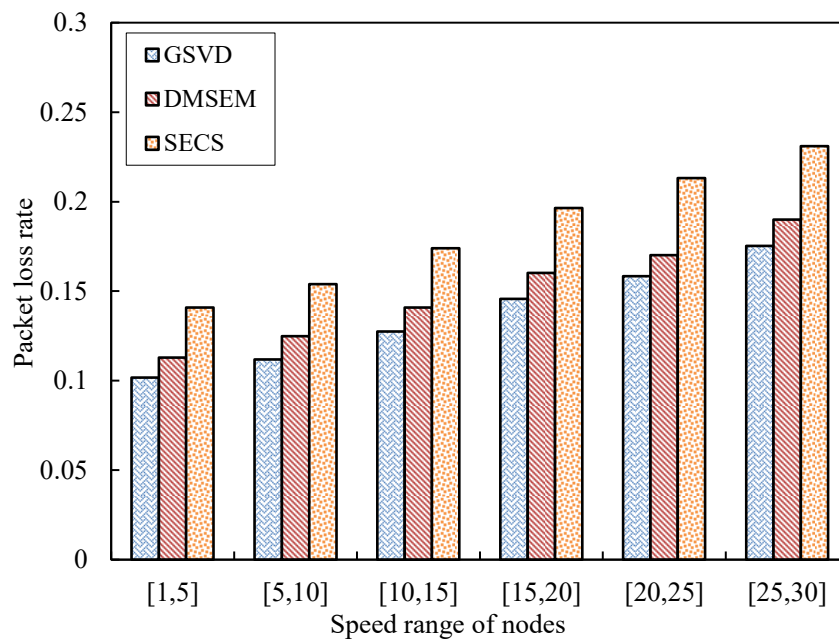
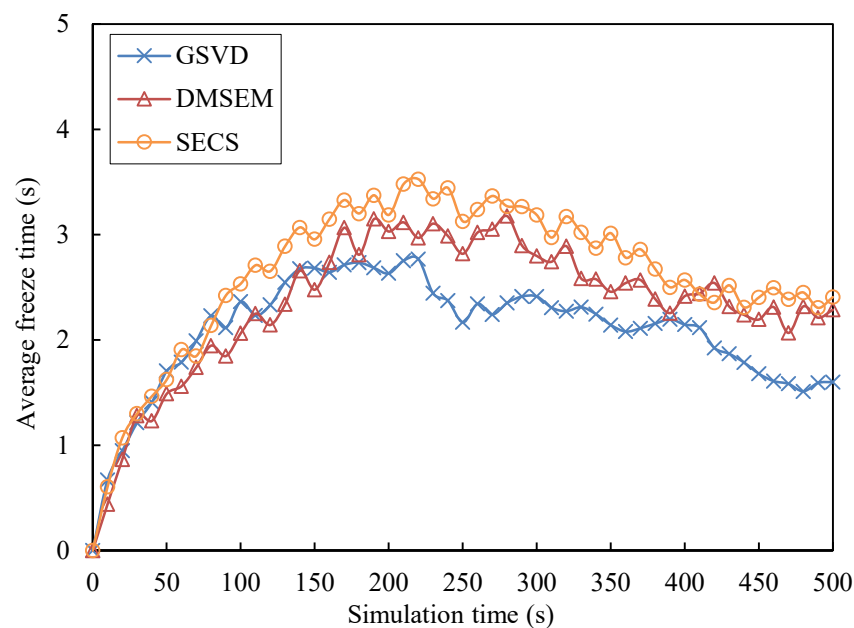


Figure 8. Packet loss rate against various speed ranges of nodes.

GSVD makes use of the code-based geographical location to calculate the geographical distance between the mobile nodes by partition of the coded grids to express the geographical location of mobile nodes. In order to reduce the negative influence levels of mobility, GSVD investigates the transmission delay and data loss rate in the process of video data delivery and estimates the video delivery quality. GSVD relies on the mobility-adapted video delivery to achieve high performance of the video data delivery by allocation of the optimal video supply node according to the estimation of delivery capacity. Once the delivery performance of video data decreases, the video request nodes reselect the optimal supply nodes. Therefore, the PLR values of GSVD is less than those of DMSEM and SECS. DMSEM investigates the encounter events between the mobile nodes to find the nodes that can share videos with one-hop D2D communications in the future. DMSEM clusters encounter events that have a similar encounter duration and a variation of geographical distance, which extracts the encounter patterns. By recognition of the encounter behaviors

of mobile nodes according to encounter patterns, DMSEM beforehand pairing with one-hop D2D communication parties is used to implement high-efficiency data delivery. The one-hop D2D communications can promote delivery performance of video data and avoid interference of path variation with multiple hops transmission. However, the mobility of mobile nodes leads to the variation of geographical distance between mobile nodes. Once the relationship of communication distance between mobile nodes changes from one-hop to multiple hops or the signal attenuates because of the lengthening geographical distance caused by mobility of mobile nodes, the risk of video data loss is greatly promoted. Therefore, the PLR values of DMSEM are severely influenced by the mobility of mobile nodes. SECS clusters the users with common interests and makes use of “pull” and “push” modes to distribute videos. Except for the intragroup video sharing based on user clustering, SECS considers economically caching distribution and management based on sharing performance awareness. However, the mobility of mobile nodes related to video data transmission cannot be considered, so that the delivery performance of video data is severely influenced by the mobility of mobile nodes and network congestion caused by intensive request. Therefore, the PLR values of SECS are higher than those of GSVD and DMSEM.

**Average freeze time (AFT):** The interruption interval time in the process of video playback of users is defined as the freeze time. The average freeze time is the ratio between the total sum of freeze time and the number of freeze during a time span  $t$ . The AFT values using  $t = 10$  s are shown in Figure 9.



**Figure 9.** Average freeze time against simulation time.

As Figure 9 shows, the three solutions maintain a fall trend after a fast rise with a slight fluctuation during the whole simulation time. The blue curve of GSVD has a fast rise from  $t = 0$  s to  $t = 130$  s and experiences a stable stage from  $t = 140$  s to  $t = 190$  s. The AFT values of GSVD also quickly fall from  $t = 200$  s to  $t = 250$  s and keep a fall with the high amplitude of fluctuation from  $t = 260$  s to  $t = 500$  s. The blue curve of GSVD is lower than those of DMSEM and SECS at most of the simulation time. The red curve of DMSEM has a fast rise from  $t = 0$  s to  $t = 170$  s and experiences a fall process from  $t = 270$  s to  $t = 500$  s after a stable stage from  $t = 180$  s to  $t = 260$  s. The orange curve of SECS has a fast fall from  $t = 230$  s to  $t = 500$  s after a fast rise from  $t = 230$  s to  $t = 500$  s. The AFT values of SECS are larger than those of GSVD and DMSEM.

As Figure 10 shows, the bars corresponding to the three solutions all have a rising trend with variation of the speed range of the nodes. The blue bars of GSVD have a slight

increase in the speed range of the nodes from [1, 5] to [5, 10] and have a fast rise from [10, 15] to [25, 30]. The AFT values of DMSEM have a slight increase in the speed range of the nodes from [1, 5] to [15, 20] and have a fast rise from [20, 25] to [25, 30]. The orange bars of SECS also have a rise trend similar to those of DMSEM and are higher than those of GSVD and DMSEM.

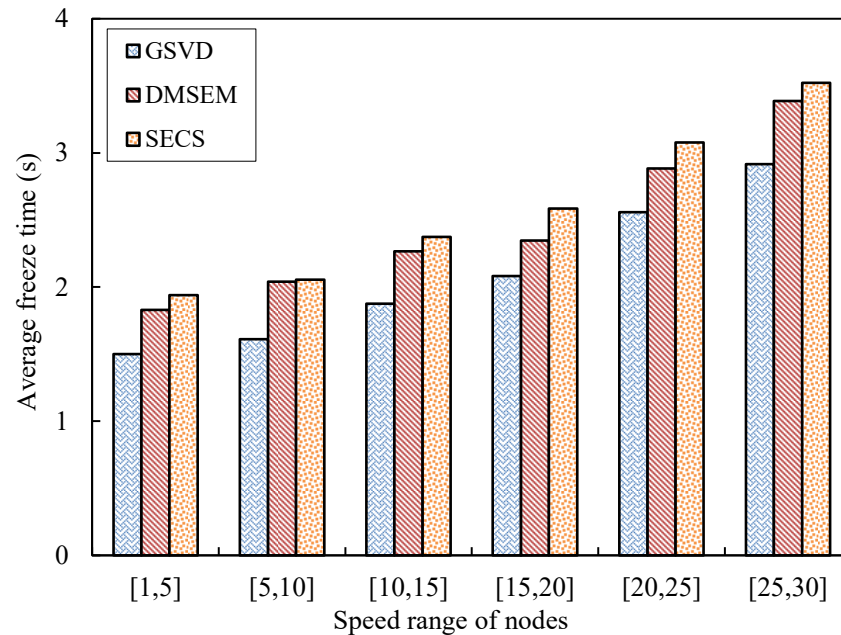


**Figure 10.** Average freeze time against the various speed ranges of the nodes.

Loss of video data and variation of the transmission delay are the main reasons of video freeze in the process of stream transmission. In order to reduce the risk of data loss and variation levels of delay, GSVD measures the video delivery quality by estimation of the transmission delay and data loss rate in the process of video data delivery. GSVD further makes use of the estimation of video delivery quality to allocate the optimal video supply nodes for the video request nodes and support the reselection supply nodes when the performance of data transmission decreases. The mobility-adapted video delivery can achieve a high performance of video data with a low delay and PLR. Therefore, the AFT values of GSVD are less than those of DMSEM and SECS. However, the fast movement of mobile nodes increases the variation levels of geographical location, which leads to a fast change of the transmission paths and bandwidth. The increasing movement speed brings a severely negative influence, so that the AFT values of GSVD rise quickly with the increasing speed of the mobile nodes. Moreover, the fast bandwidth consumption caused by the intensive request results in network congestion, which leads to an increase of PLR and transmission delay. DMSEM depends on the extracted encounter patterns to predict the encounter between the mobile nodes and pair D2D communication parties with one-hop geographical distance, which supports high-efficiency video data delivery. In order to ensure that the encounter duration meets the demand of video data transmission, DMSEM clusters the encounter events that have a similar encounter duration and variation of geographical distance. The one-hop D2D communications can promote the transmission efficiency of video data. The long-term one-hop D2D communication path also avoids interference of the path variation with multiple hops transmission. However, the fast movement of mobile nodes leads to the fragile one-hop D2D communication relationship. With the fast rise in movement speed, the fast change of geographical location increases the risk of disconnection of one-hop D2D communications. Once the geographical distance of D2D communication parties changes from one hop to multiple hops, the receivers of the video data need to re-search the new video suppliers, which prolongs the freeze time. The limited area and fast speed can promote the probabilities of the encounter of mobile

nodes, so that DMSEM has a better performance of AFT. SECS focuses on the economic caching distribution and replacement to meet the increasing demand of upload bandwidth and support the video sharing via “pull” and “push” modes. The intensive request does not bring the severely negative influence for the AFT of SECS, which has a better AFT than those of GSVD. When the large number of nodes take part into the video sharing, the fast movement of mobile nodes increases the risk of data loss and delay jitter. SECS does not consider the mobility of mobile nodes, so that the effective solutions for the performance of video data transmission caused by dynamic movement of mobile nodes cannot be formulated. The mobility of mobile nodes leads to high loss of video data and high variation levels of transmission delay, so that the AFT values of SECS increase quickly with the increasing movement speed. Therefore, the AFT values of SECS are higher than those of GSVD and DMSEM.

Peak signal-to-noise ratio (PSNR): The peak signal-to-noise ratio (PSNR) is used to denote the video quality and is measured in decibels (dB) [43]. The value of PSNR is calculated according to the equation  $PSNR = 20 \cdot \log_{10} \left( \frac{MAX\_Bit}{\sqrt{(EXP\_Thr - CRT\_Thr)^2}} \right)$ .  $EXP\_Thr$  and  $CRT\_Thr$  are the expected and real throughput, respectively.  $MAX\_Bit$  is the maximum value of transmission rate.

As Figure 11 shows, the three solutions have a fall trend with the increasing speed of the nodes. The blue bars of GSVD are higher than those of DMSEM and SECS and the decrement of PSNR values of GSVD is lower than those of DMSEM and SECS. The red bars of DMSEM have a slight fall in the speed range of the nodes from [1, 5] to [5, 10], a fast decrease from [5, 10] to [15, 20], and maintain the stable fall from [20, 25] to [25, 30]. The orange bars of SECS maintain the fast fall in the speed range of the nodes from [1, 5] to [15, 20] and have a stable fall from [20, 25] to [25, 30]. The PSNR bars of SECS are lower than those of GSVD and DMSEM.

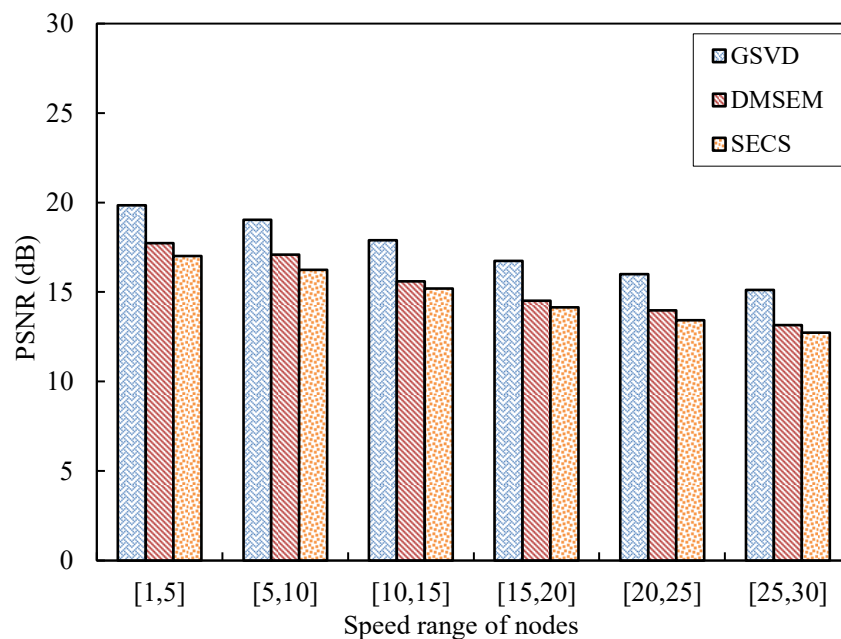


Figure 11. PSNR against various speed ranges of the nodes.

The values of PSNR are related with PLR due to the negative influence for the real throughput. GSVD depends on the mobility-adapted video delivery based on video delivery quality with the consideration of transmission delay and data loss rate to ensure the transmission performance of video data, which effectively reduces the levels and jitter of transmission delay and data loss rate. The PSNR values of GSVD are larger than those of DMSEM and SECS. DMSEM predicts the encounter between mobile nodes and pairs D2D communication parties with one-hop geographical distance by making use of the extracted encounter patterns, which obtains a high performance of video data transmission. DMSEM

clusters encounter events that have a similar encounter duration to generate the encounter patterns, which effectively reduces the negative influence of variation of geographical distance for the delivery performance of videos. Therefore, DMSEM also obtain low-level PLR. SECS does not consider the mobility of mobile nodes, so that the transmission of video data is negatively influenced by the variation of transmission paths. The PLR values of SECS are higher than those of GSVD and DMSEM. Therefore, the PSNR values of SECS are less than those of GSVD and DMSEM.

## 6. Conclusions

In this paper, we propose a novel geo-social-aware video edge delivery strategy based on modeling of the social-geographical dynamic in an urban area (GSVD). GSVD integrates social closeness, geographical distance, and video delivery quality to synthetically estimate the service capacity of video providers to guarantee the video delivery performance and user QoE. The measurement of social closeness between mobile users includes the interactive and basic social relationships. The frequency of sharing behaviors and social communication efficiency between users are used to estimate an interactive social relationship. The number of common one-hop social neighbors and the efficiency of social sub-network consisting of one-hop social neighbors of users are used to estimate basic social relationships. GSVD divides the urban area into multiple coded grids to express the geographical location of mobile users and calculate the geographical distance between mobile users. GSVD considers user QoE by estimation of the video delivery quality using two parameters: transmission delay and data loss rate. A strategy of video delivery is designed, which adapts to a social-geographical dynamic to ensure video delivery performance and user QoE. Simulation results show how GSVD achieves much better performance results in comparison with other state of the art solutions.

**Author Contributions:** Writing—original draft preparation S.J., data curation Y.C., writing—review and editing R.Z. All authors have read and agreed to the published version of the manuscript.

**Funding:** This research was funded by the Training Plan for Young Backbone Teachers of Colleges and Universities in Henan grant number 2020GGJS191, Special project of key research and development Plan of Henan Province grant number 22111111700 and Innovation Team of University Science and Technology of Henan Province grant number 22IRTSTHN016 and 23IRTSTHN017.

**Institutional Review Board Statement:** Not applicable.

**Informed Consent Statement:** Not applicable.

**Data Availability Statement:** Not applicable.

**Conflicts of Interest:** The authors declare that there is no conflict of interest regarding the publication of this paper.

## References

1. Nightingale, J.; Salva-Garcia, P.; Calero, J.M.A.; Wang, Q. 5G-QoE: QoE Modelling for Ultra-HD Video Streaming in 5G Networks. *IEEE Trans. Broadcast.* **2018**, *64*, 621–634. [[CrossRef](#)]
2. Kouhalvandi, L.; Shayea, I.; Ozoguz, S.; Mohamad, H. Overview of evolutionary algorithms and neural networks for modern mobile communication. *Trans. Emerg. Telecommun. Technol.* **2022**, *33*, e4579. [[CrossRef](#)]
3. Park, S.-H.; Jang, G.-H.; Seo, Y.-H.; Keum, H.-S.; Bang, S.-I. High-Speed Antenna Measurement System Using Multi-Probe Array Technique for 5G Applications. *Electronics* **2022**, *11*, 3435. [[CrossRef](#)]
4. Abd, A.K.; Rasool, J.M.; Rahman, Z.-A.S.A.; Al-Yasir, Y.I.A. Design and Analysis of Novel Reconfigurable Monopole Antenna Using Dip Switch and Covering 5G-Sub-6-GHz and C-Band Applications. *Electronics* **2022**, *11*, 3368. [[CrossRef](#)]
5. Ramirez, I.Q.; Sequeira, L.; Mas, J.R. An Edge-Cloud Approach for Video Surveillance in Public Transport Vehicles. *IEEE Lat. Am. Trans.* **2021**, *19*, 1763–1771. [[CrossRef](#)]
6. Xu, C.; Qin, J.; Zhang, P.; Gao, K.; Grieco, L.A. Reinforcement Learning-based Mobile AR/VR Multipath Transmission with Streaming Power Spectrum Density Analysis. *IEEE Trans. Mob. Comput.* **2021**. [[CrossRef](#)]
7. Zhong, L.; Chen, X.; Xu, C.; Ma, Y.; Wang, M.; Zhao, Y.; Muntean, G. A Multi-User Cost-Efficient Crowd-Assisted VR Content Delivery Solution in 5G-and-Beyond Heterogeneous Networks. *IEEE Trans. Mob. Comput.* **2022**. TMC.2022.3162147. [[CrossRef](#)]

8. Daz, C.; Fernandez, A.; Sacristan, F.; Garca, N. Energy- and Quality-Aware Video Request Policy for Wireless Adaptive Streaming Clients. *IEEE Trans. Consum. Electron.* **2020**, *66*, 366–375. [[CrossRef](#)]
9. Esmailyfard, R.; Esmaili, R. A privacy-preserving mechanism for social mobile crowdsensing using game theory. *Trans. Emerg. Telecommun. Technol.* **2022**, *33*, e4517. [[CrossRef](#)]
10. Agrawal, J.; Kapoor, M.; Tomar, R. A ferry mobility based direction and time-aware greedy delay-tolerant routing (FM-DT-GDR) protocol for sparse flying ad-hoc network. *Trans. Emerg. Telecommun. Technol.* **2022**, *33*, e4533. [[CrossRef](#)]
11. Xu, F.; Zhang, Z.; Feng, J.; Qin, Z.; Xie, Y. Efficient deployment of multi-UAV assisted mobile edge computing: A cost and energy perspective. *Trans. Emerg. Telecommun. Technol.* **2022**, *33*, e4453. [[CrossRef](#)]
12. Shahina, K.; Pradeep Kumar, T.S. Similarity-based clustering and data aggregation with independent component analysis in wireless sensor networks. *Trans. Emerg. Telecommun. Technol.* **2022**, *33*, e4462. [[CrossRef](#)]
13. Shen, H.; Li, Z.; Lin, Y.; Li, J. SocialTube: P2P-assisted Video Sharing in Online Social Networks. *IEEE Trans. Parallel Distrib. Syst.* **2014**, *25*, 2428–2440. [[CrossRef](#)]
14. Yan, H.; Liu, J.; Li, Y.; Jin, D.; Chen, S. Spatial Popularity and Similarity of Watching Videos in Large-Scale Urban Environment. *IEEE Trans. Netw. Serv. Manag.* **2018**, *15*, 797–810. [[CrossRef](#)]
15. Li, Y.; Wang, J.; Sun, X.; Li, Z.; Liu, M.; Gui, G. Smoothing-Aided Support Vector Machine Based Nonstationary Video Traffic Prediction Towards B5G Networks. *IEEE Trans. Veh. Technol.* **2020**, *69*, 7493–7502. [[CrossRef](#)]
16. Park, G.S.; Song, H. Cooperative Base Station Caching and X2 Link Traffic Offloading System for Video Streaming Over SDN-Enabled 5G Networks. *IEEE Trans. Mob. Comput.* **2019**, *18*, 2005–2019. [[CrossRef](#)]
17. Akhtar, M.J.; Mahum, R.; Butt, F.S.; Amin, R.; Sherbeeney, A.M.E.; Lee, S.M.; Shaikh, S. A Robust Framework for Object Detection in a Traffic Surveillance System. *Electronics* **2022**, *11*, 3425. [[CrossRef](#)]
18. Xiao, H.; Xu, C.; Ma, Y.; Yang, S.; Zhong, L.; Muntean, G. Edge Intelligence: A Computational Task Offloading Scheme for Dependent IoT Application. *IEEE Trans. Wirel. Commun.* **2022**. [[CrossRef](#)]
19. Cao, Y.; Jiang, T.; Chen, X.; Zhang, J.; Social-Aware Video Multicast Based on Device-to-Device Communications. *IEEE Trans. Mob. Comput.* **2016**, *15*, 1528–1539. [[CrossRef](#)]
20. Hu, H.; Wen, Y.; Chua, T.-S.; Huang, J.; Zhu, W.; Li, X. Joint Content Replication and Request Routing for Social Video Distribution Over Cloud CDN: A Community Clustering Method. *IEEE Trans. Circuits Syst. Video Technol.* **2018**, *26*, 1320–1333. [[CrossRef](#)]
21. Wang, X.; Chen, M.; Kwon, T.T.; Yang, L.T.; Leung, V.C.M. AMES-Cloud: A Framework of Adaptive Mobile Video Streaming and Efficient Social Video Sharing in the Clouds. *IEEE Trans. Multimed.* **2013**, *15*, 811–820. [[CrossRef](#)]
22. Alam, K.M.; Saini, M.; Ahmed, D.T.; Saddik, A.E. VeDi: A vehicular crowd-sourced video social network for VANETs. In Proceedings of the 39th Annual IEEE Conference on Local Computer Networks Workshops, Edmonton, AB, Canada, 8–11 September 2014.
23. Lin, W.S.; Zhao, H.V.; Liu, K.J.R. Cooperation Stimulation Strategies for Peer-to-Peer Wireless Live Video-Sharing Social Networks. *IEEE Trans. Image Process.* **2010**, *19*, 1768–1784. [[CrossRef](#)] [[PubMed](#)]
24. Jiao, J.; Guo, S.; Wang, Y.; Yang, Y. Energy-Efficient Cooperative Scalable Video Distribution and Sharing in Mobile Social Networks. In Proceedings of the 2019 15th International Conference on Mobile Ad-Hoc and Sensor Networks (MSN), Shenzhen, China, 11–13 December 2019.
25. Hung, Y.-H.; Wang, C.-Y.; Hwang, R.-H. Optimizing Social Welfare of Live Video Streaming Services in Mobile Edge Computing. *IEEE Trans. Mob. Comput.* **2020**, *19*, 922–934. [[CrossRef](#)]
26. Wang, M.; Xu, C.; Chen, X.; Hao, H.; Zhong, L.; Yu, S. Differential Privacy Oriented Distributed Online Learning for Mobile Social Video Prefetching. *IEEE Trans. Multimed.* **2019**, *21*, 636–651. [[CrossRef](#)]
27. Li, Z.; Wu, Q.; Salamati, K.; Xie, G. Video Delivery Performance of a Large-Scale VoD System and the Implications on Content Delivery. *IEEE Trans. Multimed.* **2015**, *17*, 880–892. [[CrossRef](#)]
28. Choi, M.; No, A.; Ji, M.; Kim, J. Markov Decision Policies for Dynamic Video Delivery in Wireless Caching Networks. *IEEE Trans. Wirel. Commun.* **2019**, *18*, 5705–5718. [[CrossRef](#)]
29. Jia, S.; Xu, C.; Guan, J.; Zhang, H.; Muntean, G.-M.; A Novel Cooperative Content Fetching-Based Strategy to Increase the Quality of Video Delivery to Mobile Users in Wireless Networks. *IEEE Trans. Broadcast.* **2014**, *60*, 370–384. [[CrossRef](#)]
30. Xiang, L.; Ng, D.W.K.; Islam, T.; Schober, R.; Wong, V.W.S.; Wang, J. Cross-Layer Optimization of Fast Video Delivery in Cache- and Buffer-Enabled Relaying Networks. *IEEE Trans. Veh. Technol.* **2017**, *66*, 11366–11382. [[CrossRef](#)]
31. Roy, S.D.; Mei, T.; Zeng, W.; Li, S. Towards Cross-Domain Learning for Social Video Popularity Prediction. *IEEE Trans. Multimed.* **2018**, *15*, 1255–1267. [[CrossRef](#)]
32. Xu, J.; Schaar, M.v.d.; Liu, J.; Li, H. Forecasting Popularity of Videos Using Social Media. *IEEE J. Sel. Top. Signal Process.* **2015**, *9*, 330–343. [[CrossRef](#)]
33. Yang, W.; Ma, J.; Li, Y.; Yan, R.; Yuan, J.; Wu, W.; Li, D. Marginal Gains to Maximize Content Spread in Social Networks. *IEEE Trans. Comput. Soc. Syst.* **2019**, *6*, 479–490. [[CrossRef](#)]
34. Niu, G.; Fan, X.; Li, V.O.K.; Long, Y.; Xu, K. Multi-Source-Driven Asynchronous Diffusion Model for Video-Sharing in Online Social Networks. *IEEE Trans. Multimed.* **2014**, *16*, 2025–2037. [[CrossRef](#)]
35. Fan, Y.; Yang, B.; Hu, D.; Yuan, X.; Xu, X. Social- and Content-Aware Prediction for Video Content Delivery. *IEEE Access* **2020**, *8*, 29219–29227. [[CrossRef](#)]

36. Zhang, R.; Jia, S.; Ma, Y.; Xu, C. Social-Aware D2D Video Delivery Method Based on Mobility Similarity Measurement in 5G Ultra-Dense Network. *IEEE Access* **2020**, *8*, 52413–52427. [[CrossRef](#)]
37. Wang, Z.; Liu, J.; Zhu, W. Social-aware video delivery: Challenges, approaches, and directions. *IEEE Netw.* **2016**, *30*, 35–39. [[CrossRef](#)]
38. Jia, S.; Zhou, Z.; Li, W.; Ma, Y.; Zhang, R.; Wang, T. Social-Aware Edge Caching Strategy of Video Resources in 5G Ultra-Dense Network. *Mob. Inf. Syst.* **2021**, *2021*, 6625629. [[CrossRef](#)]
39. Li, W. Random texts exhibit Zipf’s-law-like word frequency distribution. *IEEE Trans. Inf. Theory* **1992**, *38*, 1842–1845. [[CrossRef](#)]
40. Li, Q.; Zhang, Y.; Pandharipande, A.; Ge, X.; Zhang, J. D2D-Assisted Caching on Truncated Zipf Distribution. *IEEE Access* **2019**, *7*, 13411–13421. [[CrossRef](#)]
41. Aldalbahi, A.; Rahaim, M.; Khreishah, A.; Ayyash, M.; Little, T.D.C. Visible Light Communication Module: An Open Source Extension to the ns3 Network Simulator With Real System Validation. *IEEE Access* **2017**, *5*, 22144–22158. [[CrossRef](#)]
42. Zhang, H.; Liao, Y.; Song, L. D2D-U: Device-to-Device Communications in Unlicensed Bands for 5G System. *IEEE Trans. Onwireless Commun.* **2017**, *16*, 3507–3519. [[CrossRef](#)]
43. Lee, S.-B.; Muntean, G.-M.; Smeaton, A.F. Performance-aware replication of distributed pre-recorded IPTV content. *IEEE Trans. Broadcast.* **2009**, *55*, 516–526.